Asymmetric resonance frequency analysis of in-plane electrothermal silicon cantilevers for nanoparticle sensors

Maik Bertke[1,2,*], Gerry Hamdana[1,2], Wenze Wu[1,2], Markus Marks[1], Hutomo Suryo Wasisto[1,2] and Erwin Peiner[1,2]

[1] Institute of Semiconductor Technology (IHT), Braunschweig University of Technology, Hans-Sommer-Straße 66, D-38106 Braunschweig, Germany
[2] Laboratory for Emerging Nanometrology (LENA), Langer Kamp 6a, D-38106 Braunschweig, Germany

[*]E-mail: M.Bertke@tu-bs.de

Abstract. The asymmetric resonance frequency analysis of silicon cantilevers for a low-cost wearable airborne nanoparticle detector (Cantor) is described in this paper. The cantilevers, which are operated in the fundamental in-plane resonance mode, are used as a mass-sensitive microbalance. They are manufactured out of bulk silicon, containing a full piezoresistive Wheatstone bridge and an integrated thermal heater for reading the measurement output signal and stimulating the in-plane excitation, respectively. To optimize the sensor performance, cantilevers with different cantilever geometries are designed, fabricated and characterized. Besides the resonance frequency, the quality factor (Q) of the resonance curve has a high influence concerning the sensor sensitivity. Because of an asymmetric resonance behaviour, a novel fitting function and method to extract the Q is created, different from that of the simple harmonic oscillator (SHO). For testing the sensor in a long-term frequency analysis, a phase-locked loop (PLL) circuit is employed, yielding a frequency stability of up to 0.753 Hz at an Allan variance of 3.77×10^{-6}. This proposed asymmetric resonance frequency analysis method is expected to be further used in the process development of the next-generation Cantor.

1. Introduction

Since the last few years, more and more types of nanoparticles (NPs) have been used in different consumer goods, resulting in an increasing awareness towards releasing these NPs in air. Because of their small size, possessed hazard, and presence in both indoor and outdoor environments, they can become a huge danger or risk when they are exposed to human body via either direct deposition on the skin or inhalation through respiratory systems [1]. Therefore, there have been many studies concerning the characteristics and health effects of different types of airborne NPs in the environmental communities as well as the strategies to manage their exposure [2].

To ensure a safety of the workers who directly handle and interact with NPs during the manufacturing of the NP-based devices or products, it is necessary to equip them with a low-cost wearable direct-reading tool for continuously monitoring the airborne NP mass concentration levels [3]. Therefore, owing to their detection simplicity and cost-effective batch fabrication, various types of resonant micro/nanoelectromechanical systems (M/NEMS) were developed as NP mass-sensitive sensors by several world-leading research groups to meet the demands (e.g., microfluidic film bulk acoustic resonator (FBAR) [4], electrothermal silicon cantilever [5], filter-fiber nanoresonator [6], and vertical silicon nanowire resonator [7]). The NP measurement principle is based on the monitoring of the

resonance frequency shifts of the M/NEMS caused by the NPs additionally deposited on their surfaces. In our second generation of the pocket-sized *can*tilever-based airborne NP detec*tor* (Cantor-2), the in-plane electrothermal piezoresistive silicon cantilever is connected to a phase-locked loop (PLL) circuit to realize a real-time tracking system of the resonance frequency [8, 9]. However, the phenomenon of the asymmetric resonance frequency signals produced by the employed cantilevers has not been analyzed in details. Thus, in this work, several designs of the electrothermal cantilever resonators are investigated in terms of their resonance characteristics, which will then be used as a basis for further improvement of the Cantor. Moreover, their frequency stability is also measured to define the Allan variance of the device in a long-term test.

2. Sensor preparations

The electrothermal silicon cantilever resonators with different free-end geometries (Figures 1(a)-(d)) were simulated using the finite element modelling (FEM) tool of COMSOL Multiphysics 4.3b to determine their figure of merit (i.e., $FoM = m_c/(f_0 \times A_c \times Q)$ [10]) as listed in Table 1. In this case, m_c, f_0, and A_c denote the mass of the cantilever, the resonance frequency, and the area of the collection surface, respectively. It should be noted that all these cantilevers have a total length of 1000 µm and a beam spring width of 170 µm. By exciting the heating resistor on the cantilever with a DC bias of 5 V, the temperature (T) increases from 293.15 K to 306.1 K (i.e., $\Delta T = 12.95$ K) resulting in a cantilever bending (Figure 2(a)). The calculated maximum stress obtained from FEM is 3.63×10^7 N/m^2 [9].

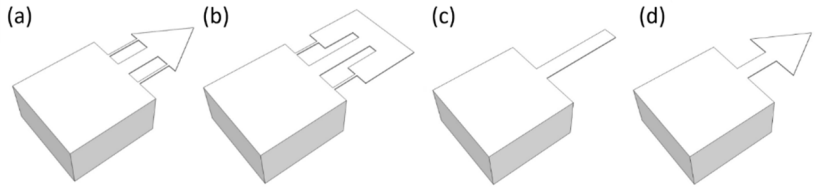

Figure 1. Designs of (a) a triangular cantilever with strivings (C_{ts}), (b) a rectangular cantilever with strivings (C_{rs}), (c) a rectangular cantilever (C_s), and (d) a triangular cantilever (C_t).

Table 1. FEM results of four cantilever resonators with different free-ends.

Cantilever	f_0 [kHz]	A_c [mm^2]	m_c [µg]	Q	FoM
C_{ts}	351,380	0.248	7.80	9497	9.4×10^{-9}
C_{rs}	166,228	0.570	17.92	5541	3.4×10^{-8}
C_s	217,150	0.139	4.37	4343	3.3×10^{-8}
C_t	185,329	0.248	7.80	3497	4.9×10^{-8}

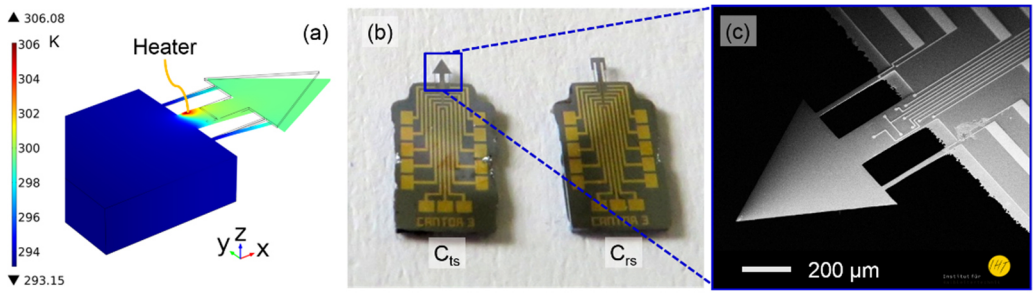

Figure 2. (a) 3-D FEM result, (b) photograph, and (c) scanning electron micrograph of one of the fabricated sensors (i.e., the triangular cantilever with strivings C_{ts}).

Subsequently, these in-plane cantilevers were fabricated using bulk silicon wafers and bulk micromachining techniques, leading to lower cost of materials and fabrication processes, respectively (Figures 2(b) and (c)). The detailed fabrication steps have been described previously, which mainly employ photolithography, dopant diffusions using borofilm 100 and phosphorosilica (Emulsitone), thermal oxidation, metal evaporation, and inductively coupled plasma (ICP) cryogenic dry etching processes [9].

3. Resonance frequency analysis

To analyze the resonance behaviors of the fabricated cantilevers (Figures 3(a)-(d)), a frequency sweep was carried out using the measurement setup described in [10]. The main relevant parameters of the measured resonance curves are the f_0, the Q and the relative amplitude of the peak, which can be directly extracted from a fitting procedure. Because of the asymmetry of the resonance curve, a fitting function in relation to the Fano resonance is developed replacing the commonly used simple harmonic oscillator (SHO) fitting function [11]. The Fano resonance is based on a system of two coupled vibrations where one is forced to its oscillation directly and their superposition will result in an asymmetric resonance behavior (Figure 4) [12].

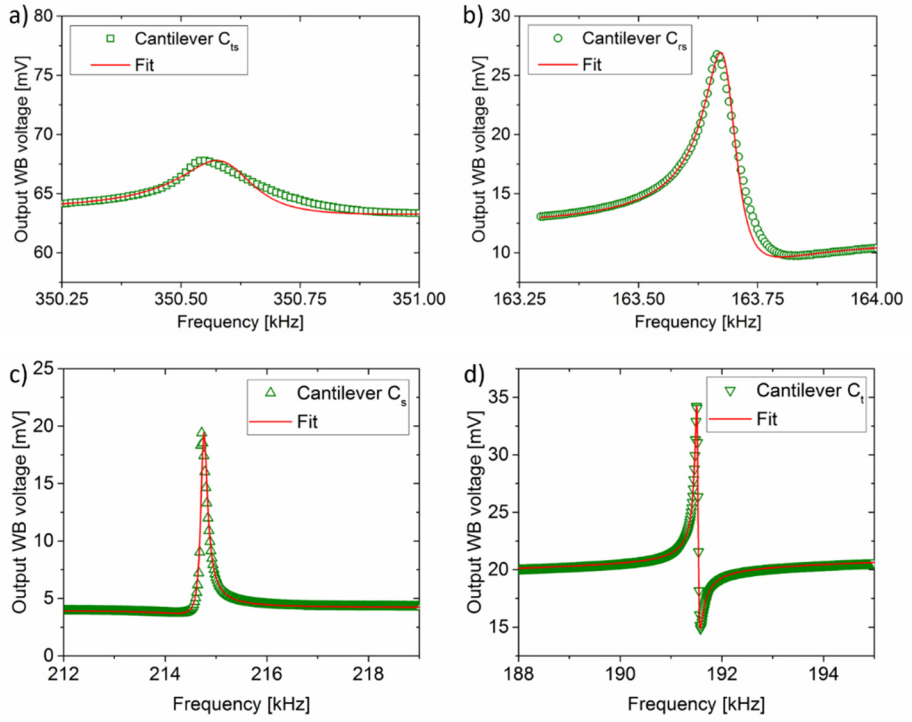

Figure 3. Measured resonance curves of cantilevers and their corresponding fittings of (a) C_{ts}, (b) C_{rs}, (c) C_s, and (d) C_t.

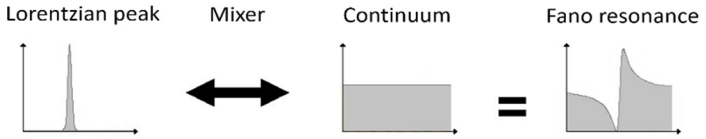

Figure 4. Illustration of a Fano resonance as a mixed combination of a discrete state and a continuous background.

The Fano resonance frequency response can be described implicitly by [12]:

$$\frac{q^2-1}{f^2+1}+\frac{2qf}{f^2+1}+1=\frac{(f+q)^2}{f^2+1}, \tag{1}$$

where q and f are the asymmetry factor and the frequency, respectively. The frequency sweep response σ around the f_0 is then given by:

$$\sigma=\frac{\left(\frac{f-f_0}{g}+q\right)^2}{\left(\frac{f-f_0}{g}\right)^2+1}\times H+\sigma_0+t\times f \tag{2}$$

with line width and gain parameters g and H, respectively, and an offset comprising a constant (σ_0) and linearly varying term ($t \times f$). The proposed Q is calculated by combining two established methods (i.e., $Q_{q=0} = f_0/2g[(2)^{0.5}\text{-}1]^{0.5}$ and $Q_{q=1} = (2f_0^2+2g^2)/(4g\times f_0)$ [13]) with their newly introduced correction factors of $(1\text{-}|q|^{0.5})$ and $|q|^{0.5}$ as:

$$Q=\frac{f_0}{2g\sqrt{\sqrt{2}-1}}\left(1-\sqrt{|q|}\right)+\frac{2f_0^{\,2}+2g^2}{4g\times f_0}\sqrt{|q|}\ \text{ for } q=\pm 0\ldots 1\,. \tag{3}$$

A simulation of an electrical RLC circuit using MATLAB is used as a reference to validate Equation (3) replicating the different resonance curves. In this case, an excitation is generated to bring the circuit to resonance followed by a cut off at steady state. The yielded decaying response amplitude can then be fitted over the time. The damping of the oscillation defines the quality factor of the system [13,14]. Figures 5(a)-(c) depict the resonance curves with different asymmetry levels calculated using Equation (2). For the validation, the frequency responses of the fitted RLC circuit are added. The relative deviation between the calculated and simulated f_0 and Q are listed in Table 2. Small differences between these two curves (Figure 5(a)) causes the deviation of f_0 and Q at $q = 1$. We find that inaccuracies of the Equation (3) at $q = 0.5$ and $q = 0.25$ are still comparable with that of $q = 1$ (i.e., $\Delta Q < 0.7$), proving its reliability.

Table 2. The relative deviation between the calculated and simulated validation results of the f_0 and Q in terms of the quality of developed Equation (3).

Asymmetry factor	$\Delta f_0/f_0$	$\Delta Q/Q$
$q = 1$	3.03×10^{-4}	6.8×10^{-3}
$q = 0.5$	2.01×10^{-4}	13.6×10^{-3}
$q = 0.25$	4.01×10^{-4}	4.2×10^{-3}

Table 3. Comparison of the f_0 and Q obtained from measurement and FEM.

Cantilever	$f_{0\_measured}$ [Hz]	$Q_{\_measured}$	f_{0_FEM} [Hz]	$Q_{\_FEM}$
C_{ts}	350,595 ± 2	2401 ± 48	351,380	9497
C_{rs}	163,687 ± 1	2491 ± 57	166,228	5541
C_s	214,755 ± 4	2087 ± 95	217,150	4343
C_t	191,530 ± 1	3242 ± 43	185,329	3497

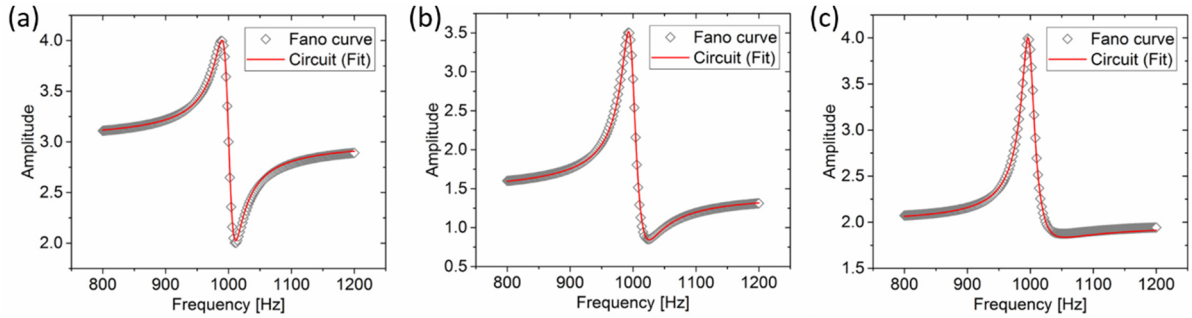

Figure 5. Fitting analysis of the Fano resonance and the RLC circuit curves for verifying the quality of the developed Equation (3) for (a) $q = 1$, (b) $q = 0.5$ and (c) $q = 0.25$.

Furthermore, Table 3 shows good agreement of the f_0 obtained from FEM and the fitting of the measurements with four different cantilever sensors using Equations (2) and (3). However, the Q values of the designed cantilevers with strivings (C_{ts} and C_{rs}) are much lower than expected, which can be due to the simplification of the 3-D model geometries used in the FEM.

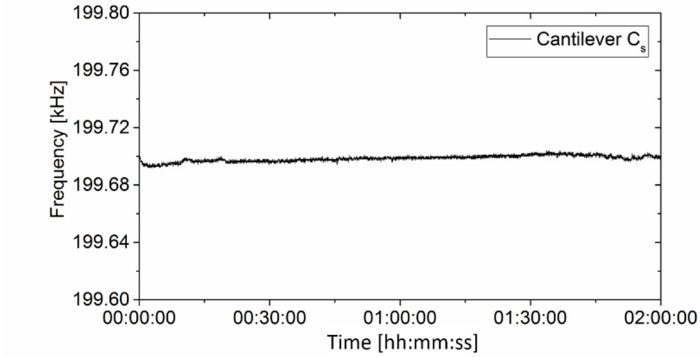

Figure 6. Measurement result of the long-term stability of a cantilever resonator with PLL-based tracking electronics.

Moreover, in the long-term stability tests using a homebuilt PLL circuit [15], the fabricated cantilevers without strivings (C_s and C_t) have demonstrated a frequency stability of up to 0.753 Hz at an Allan variance of 3.77×10^{-6} (Figure 6). Although the proposed sensors have shown promising results in terms of the simulation and measurement (i.e., high $Q > 2000$), some geometry modifications as well as fabrication parameter adjustments are still required to enhance the performance of the devices. Besides that, the described asymmetric resonance frequency fitting method (i.e., based on Fano resonance method) is expected to be employed supporting the optimization of the next-generation Cantors to precisely estimate their resonance characteristics (i.e., f_0 and Q).

4. Conclusions

Electrothermal silicon piezoresistive cantilever sensors with different free-end geometries have been analyzed in terms of their asymmetric resonance behaviors. A novel fitting model based on the Fano resonance approach has been developed to precisely extract the values of the resonance frequency and quality factor (Q) of the devices, replacing the simple harmonic oscillator (SHO) fitting model. Moreover, despite the promising results from long-term stability tests, further experiments of the cantilever resonators in airborne nanoparticle (NP) exposure are still needed to justify the resonance characteristics of the devices in the conditions of before and after being polluted with NPs.

References

[1] Pini M, Salieri B, Ferrari A M, Nowack B and Hischier R 2016 Human health characterization factors of nano-TiO_2 for indoor and outdoor environments *Int. J. Life Cycle Assess* 1-11 http://dx.doi.org/10.1007/s11367-016-1115-8.

[2] Díaz-Soler B M, Martínez-Aires M D and López-Alonso M 2016 Emerging risk in the construction industry: Recommendations for managing exposure to nanomaterials *DYNA* **83**(196), 48-54, http://dx.doi.org/10.15446/dyna.v83n196.56608.

[3] Kuhlbusch T A J, Asbach C, Fissan H, Göhler D and Stintz M 2011 Nanoparticle exposure at nanotechnology workplaces: A review *Particle and Fibre Toxicology* **8**(22) 1-18 http://dx.doi.org/10.1186/1743-8977-8-22.

[4] Paprotny I, Doering F, Solomon P A, White R M and Gundel L A 2013 Microfabricated air-microfluidic sensor for personal monitoring of airborne particulate matter: Design, fabrication, and experimental results *Sens. Actuators A Phys.* **201** 506–16 http://dx.doi.org/10.1016/j.sna.2012.12.026.

[5] Beardslee L A, Addous A M, Heinrich S, Josse F, Dufour I and Brand O 2010 Thermal excitation and piezoresistive detection of cantilever in-plane resonance modes for sensing applications *J. Microelectromech.* **19** 1015–17 http://dx.doi.org/10.1109/JMEMS.2010.2052093.

[6] Schmid S, Kurek M, Adolphsen J Q and Boisen A 2013 Real-time single airborne nanoparticle detection with nanomechanical resonant filter-fiber *Scientific Reports* **3** 1288 http://dx.doi.org/10.1038/srep01288.

[7] Wasisto H S, Merzsch S, Stranz A, Waag A, Uhde E, Salthammer T and Peiner E 2013 Femtogram aerosol nanoparticle mass sensing utilising vertical silicon nanowire resonators *Micro Nano Lett.* **8**(10) 554–8 http://dx.doi.org/10.1049/mnl.2013.0208.

[8] Wasisto H S, Uhde E and Peiner E 2016 Enhanced performance of pocket-sized nanoparticle exposure monitor for healthy indoor environment *Build. Environ.* **95** 13–20 http://dx.doi.org/10.1016/j.buildenv.2015.09.013.

[9] Wasisto H S, Merzsch S, Uhde E, Waag A and Peiner E 2015 Handheld personal airborne nanoparticle detector based on microelectromechanical silicon resonant cantilever *Microelectron. Eng.* **145** 96–103 http://dx.doi.org/10.1016/j.mee.2015.03.037.

[10] Wasisto H S, Wu W, Uhde E, Waag A and Peiner E 2015 Electrothermal piezoresistive cantilever resonators for personal measurements of nanoparticles in workplace exposure *Proc. SPIE 9517, Smart Sensors, Actuators, and MEMS VII, and Cyber Physical Systems* **95170**B http://dx.doi.org/10.1117/12.2180151.

[11] Wasisto H S, Merzsch S, Waag A, Uhde E, Salthammer T and Peiner E 2013 Airborne engineered nanoparticle mass sensor based on a silicon resonant cantilever *Sens. Actuator B Chem.* **180** 77–89 http://dx.doi.org/10.1016/j.snb.2012.04.003.

[12] Miroshnichenko A E, Flach S and Kivshar Y S 2010 Fano resonances in nanoscale structures *Rev. Mod. Phys.* **82** 2257–98 http://dx.doi.org/10.1103/RevModPhys.82.2257.

[13] Manzaneque T, Hernando H and Rodríguez-Aragón L 2010 Analysis of the quality factor of AlN-actuated micro-resonators in air and liquid *Microsyst. Technol.* **16** 837-45 http://dx.doi.org/10.1007/s00542-009-1003-2.

[14] Toledo J, Manzaneque T, Hernando-García J and Vázquez J 2014 Application of quartz tuning forks and extensional microresonators for viscosity and density measurements in oil/fuel mixtures *Microsyst Technol.* **20**(4) 945–53 http://dx.doi.org/10.1007/s00542-014-2095-x.

[15] Wasisto H S, Zhang Q, Merzsch S, Waag A and Peiner E 2014 A phase-locked loop frequency tracking system for portable microelectromechanical piezoresistive cantilever mass sensors *Microsyst. Technol.* **20**(4), 559–69 http://dx.doi.org/10.1007/s00542-013-1991-9.